Contrib Mineral Petrol (1995) 121:87–98

Alan B. Woodland · Hugh St. C. O'Neill

Phase relations between $Ca_3Fe_2^{3+}Si_3O_{12}$–$Fe_3^{2+}Fe_2^{3+}Si_3O_{12}$ garnet and $CaFeSi_2O_6$–$Fe_2Si_2O_6$ pyroxene solid solutions

Received: 11 November 1994/Accepted: 3 April 1995

The stability of Ca-bearing garnets on the join $Ca_3Fe_2^{3+}Si_3O_{12}$–$Fe_3^{2+}Si_3O_{12}$ (andradite – "skiagite") has been investigated as a function of pressure at 1100° C. The experiments were performed using a series of glasses and slags with fixed Fe^{3+}/Fe_{total} in a piston cylinder apparatus and a multi-anvil press. The maximum solubility of "skiagite" in andradite increases from 12 mol% at 1.7 GPa to 48 and 64 mol% at 6.0 and 7.0 GPa respectively. This is greater than that found for the solubility of "skiagite" in almandine ($Fe_3^{2+}Al_2Si_3O_{12}$) garnet at the same pressure and temperature conditions. The equilibrium garnet solid solutions at 1100° C coexist with spinel + clinopyroxene + quartz or coesite at $0.7 < P < 7.0$ GPa. Above 7.0 GPa garnet may coexist with either spinel + clinopyroxene + coesite or with Fe_2SiO_4-rich spinel + coesite depending on the bulk Fe^{3+}/Fe_{total}. The coexisting clinopyroxene becomes progressively more Fe-rich with increasing pressure until a miscibility gap is intersected at 7.0 GPa. Above this pressure, the pyroxenes are Ca-poor and monoclinic (space group $P2_1/c$), but probably have the C2/c space group at the conditions of the experiments. There is a highly asymmetric miscibility gap between this Ca-poor high pressure form and the hedenbergite–clinoferrosilite solid solution, similar to that formed between Ca-poor orthopyroxene and hedenbergite solid solutions at lower pressures. Determination of the mixing properties of the garnet solid solutions and the $\Delta_f G^{\circ}_{1373K,1bar}$ for "skiagite" can potentially be determined from the Ca-Fe^{2+} exchange between garnet and pyroxene. However this analysis is hampered by problems in modelling the properties of the coexisting clinopyroxene.

Alan B. Woodland (✉)[1] · Hugh St.C. O'Neill[2]
Bayerisches Geoinstitut, Universität Bayreuth. D-95440 Bayreuth, Germany
[1]*now at*: Mineralogisch-Petrographisches Institut, Universität Heidelberg, Im Neuenheimer Feld 236, D-69120 Heidelberg, Germany
[2]*now at*: Research School of Earth Sciences, Australian National University, Canberra, ACT 0200, Australia

Editorial responsibility: J. Hoefs

Introduction

Garnets containing both Fe^{2+} and Fe^{3+} are potentially useful as monitors of oxygen fugacity in upper mantle rocks (e.g., Luth et al. 1990; Gudmundsson and Wood 1995). However, at present, the accuracy of potential garnet oxygen geobarometers is limited by our incomplete knowledge of the thermodynamic mixing properties of compositionally complex Fe^{2+}- and Fe^{3+}-containing garnets. In particular, there are expected to be contributions to the Gibbs free energy of mixing in the garnet solid solution from reciprocal solution effects (e.g. Wood and Nicholls 1978) as well as from possible non-ideal mixing behaviour on the dodecahedral or octahedral sites. To account for these effects in most natural garnet compositions, the properties of the three Fe^{3+}-bearing components: ($Ca_3Fe_2^{3+}Si_3O_{12}$), andradite, ($Fe_3^{2+}Fe_2^{3+}Si_3O_{12}$), skiagite, and ($Mg_3Fe_2^{3+}Si_3O_{12}$), khoharite and their mutual solid solution behaviour need to be determined. Although the name skiagite has been discredited as a mineral name we retain its usage here to refer to an end-member component that can be present in complex garnet solid solutions. Because of the reciprocal solution effect the properties of $Fe_3^{2+}Fe_2^{3+}Si_3O_{12}$ must be considered even when reactions not explicitly containing this end-member are used. An example of such a reaction which is a potential oxygen barometer for garnet lherzolites is (Luth et al. 1990):

$$Ca_3Fe_2^{3+}Si_3O_{12} + 3Mg_2Si_2O_6 + 2Fe_2Si_2O_6 = 6CaMgSi_2O_6 + 4Fe_2SiO_4 + O_2$$

The activity of the $Ca_3Fe_2^{3+}Si_3O_{12}$ component in the complex garnet solid solution depends on the properties of the $Fe_3^{2+}Fe_2^{3+}Si_3O_{12}$ and $Mg_3Fe_2^{3+}Si_3O_{12}$ components through the two reciprocal reactions:

$$Ca_3Fe_2^{3+}Si_3O_{12} + Fe_3^{2+}Al_2Si_3O_{12} = Fe_3^{2+}Fe_2^{3+}Si_3O_{12} + Ca_3Al_2Si_3O_{12} \quad (1)$$

$$Ca_3Fe_2^{3+}Si_3O_{12} + Mg_3Al_2Si_3O_{12} = Mg_3Fe_2^{3+}Si_3O_{12} + Ca_3Al_2Si_3O_{12} \quad (2)$$

As a first step in obtaining the thermodynamic data needed to model complex garnet solid solutions, the $\Delta_f G^0$ for skiagite was determined by Woodland and O'Neill (1993) at 1100° C from the exchange reaction between $Fe_3^{2+}Al_2Si_3O_{12}$–$Fe_3^{2+}Fe_2^{3+}Si_3O_{12}$ (almandine–skiagite) garnet solid solutions and coexisting spinel solid solutions.

In this study, we extend our investigation of Fe^{2+}–Fe^{3+} garnet solid solutions by determining the stability of Ca-bearing garnets on the join $Ca_3Fe_2^{3+}Si_3O_{12}$–$Fe_3^{2+}Fe_2^{3+}Si_3O_{12}$ (andradite-skiagite) as a function of pressure at 1100° C. Our goals are to: (1) determine the extent of Ca-Fe^{2+} mixing on the dodecahedral site in the presence of octahedral Fe^{3+}; (2) assess the possibility of non-ideal behaviour in these solid solutions; (3) determine the relations between garnet and coexisting phases such as spinel and pyroxenes in the system CaO-FeO-Fe_2O_3-SiO_2. During the course of this study we encountered a new miscibility gap in high pressure $CaFeSi_2O_6 - Fe_2Si_2O_6$ clinopyroxenes. Consequently, a subsidiary feature of this study is the determination of this miscibility gap as a function of pressure at 1100° C.

Nearly pure end-member andradite is stable over a wide range of temperatures and pressures. Its stability and thermodynamic properties have been investigated by many workers (Huckenholz and Yoder 1971; Gustafson 1974; Liou 1974; Suwa et al. 1976; Taylor and Liou 1978; Robie et al., 1987). Although inconsistencies remain between the various studies (cf. Zhang and Saxena, 1991), the properties are sufficiently well constrained for andradite to have been incorporated into several thermodynamic data bases (Moecher et al. 1988; Holland and Powell 1990).

Experimental methods

Apparatus and techniques

Experiments in the pressure range of 1.3 to 5.0 GPa were conducted in a piston cylinder apparatus, using talc-Pyrex pressure cells with diameters of 1.905 cm and 1.270 cm depending on the desired pressure. The experimental methods are the same as those reported in Woodland and O'Neill (1993). The uncertainty in pressure is estimated to be ≈0.1 GPa based upon the width of our calibration brackets. The duration of the experiments was usually between 40 and 100 hours. The starting materials were ground under acetone in an agate mortar and packed in thick-walled (0.5 mm) 3.5 mm or 5 mm Ag capsules which were sealed by hammering a friction fitting lid in place. Silver was chosen as the capsule material because the solubility of Fe in Ag is very slight (Massalski et al. 1986) and Ag is relatively impervious to H_2 (Chou 1986). This is an important consideration since diffusion of H_2 into or out of the capsule during the experiment could change the oxygen content of the solid and, therefore, the $Fe^{3+}/\Sigma Fe$ ratio of the sample. Most experiments were conducted at 1100° C, however, below ≈3.0 GPa the experiments were run at 1080° C to avoid melting the Ag capsules. Several experiments at low pressure were performed with Au capsules in order to reach 1100° C without melting the capsule material. Although Fe shows significant solubility in Au, loss of Fe to Au is expected to be minimal at the relatively oxidising conditions of our experiments with andradite-rich compositions.

Experiments between 5.5 and 10.0 GPa were run in the Sumitomo 1200 multi-anvil press at the Bayerisches Geoinstitut using Toshiba F grade WC cubes with an 11 mm truncated edge. The methods follow those described in Woodland and O'Neill (1993). The accuracy in pressure is estimated to be ± 0.3 GPa based on the width of the reversal brackets and from repeated checks of these reactions. The capsules for the multi-anvil press experiments were made from 1.7 mm Ag tubing. The ends were sealed by inserting a silver disc followed by crimping and hammering, which produced a cold weld. The duration of the multi-anvil experiments was 12 to 14.5 hours.

Starting materials

In the experimental study of redox reactions, it is necessary to control either oxygen fugacity (f_{O_2}) or oxygen content (i.e. fixed $Fe^{3+}/\Sigma Fe$ ratios). Since control of f_{O_2} is impractical in the multi-anvil experiments, we decided on the latter option with analysis of the $Fe^{3+}/\Sigma Fe$ ratio in the run products. In order to obtain garnet solid solutions with the correct stoichiometry, the $Fe^{3+}/\Sigma Fe$ ratio must be set in the starting materials. The $Fe^{3+}/\Sigma Fe$ ratio varies from 1.0 in andradite (only Fe^{3+} is present) to 0.40 for skiagite (both Fe^{3+} and Fe^{2+} are present). Following our experience with the synthesis of almandine - skiagite solid solutions, where oxide mixes yielded heterogeneous disequilibrium assemblages, we chose to use glasses or slags as starting materials. The glasses or slags were prepared by melting stoichiometric amounts of Fe_2O_3, CaO, and SiO_2 in Pt crucibles. The crucibles were presaturated with Fe prior to the syntheses in order to minimise loss of Fe from the oxide mix. The value of f_{O_2} that would yield the correct $Fe^{3+}/\Sigma Fe$ for the different compositions was estimated from diagram no. 6902 in Roth et al. (1987, p. 454–456). The relatively oxidising conditions necessary to produce the desired $Fe^{3+}/\Sigma Fe$ ratio required two different approaches to be taken. Compositions with $X_{ski} < 0.25$ were produced in air at different temperatures (between 1450° C and 1550° C) in order to vary the $Fe^{3+}/\Sigma Fe$ ratio of the glasses. For compositions with $X_{ski} > 0.25$, the correct $Fe^{3+}/\Sigma Fe$ ratio was achieved by controlling the f_{O_2} of the furnace atmosphere using Ar-O_2 gas mixes. Black-brown non-magnetic glasses were obtained up to compositions of 70 mol% andradite–30 mol% skiagite (ski30). However, at more Fe-rich compositions, quenching a glass became increasingly difficult and a magnetic vitreous slag resulted. The $Fe^{3+}/\Sigma Fe$ ratios of the andradite-rich glasses were checked by wet chemistry. Several of the glasses were found to be within 5% of the nominal values, but several others had higher Fe^{2+} contents on the order of 25% from their ideal compositions. The glasses with reduced compositions were considered to be useful since they should have produced a garnet with the maximum skiagite content for the given temperature and pressure of the experiment. The glasses were also checked by Mössbauer spectroscopy. The resulting $Fe^{3+}/\Sigma Fe$ values were found to be sensitive to the scheme used for fitting the spectra, but, the range in values obtained was in agreement with the nominal

ratio. The slags were not checked by either method because of the difficulty in completely dissolving oxide phases without causing oxidation and therefore spuriously high Fe^{3+} contents (Lucas et al., 1989), and the presence of multiple phases would make any Mössbauer spectrum virtually impossible to interpret in a quantitative fashion. The fact that the $Fe^{3+}/\Sigma Fe$ ratios is very sensitive to f_{O_2} in our desired range made it difficult to be certain that the intended stoichiometry was always attained; according to Roth et al. (1987) less than 2 log units in f_{O_2} separates a $Fe^{3+}/\Sigma Fe$ of 0.97 and 0.40 (ski10–ski100). However, since a number of the slag starting materials produced homogeneous garnets either as a single phase or with only a trace of additional phases, this indicates that the actual $Fe^{3+}/\Sigma Fe$ of most of the slags must have been close to the intended values.

End-member andradite was produced both from a glass and a stoichiometric mixture of $CaSiO_3$ and Fe_2O_3. The $CaSiO_3$ was synthesised in air at 1350° C from a mixture of $CaCO_3$ and SiO_2. The $CaSiO_3$-Fe_2O_3 mixture was then recrystallised at 1100° C and 2.8 GPa. The synthesis using the glass starting material was performed at high temperature and pressure in the piston cylinder apparatus (1300° C, 1.4 GPa) in a Pt capsule using PtO_2 to maintain a high f_{O_2} and oxidise any Fe^{2+} that may have been initially present in the glass (Huckenholz and Yoder 1971). Details of the synthesis of end-member skiagite are given in Woodland and O'Neill (1993).

Experiments to determine the extent of miscibility in the system $CaFeSi_2O_6$–$Fe_2Si_2O_6$ were performed using a mixture of $CaSiO_3$, Fe_2SiO_4, and SiO_2. The fayalite was produced at 1 bar and 1100° C in a controlled atmosphere furnace using a CO_2/CO ratio of 1/4 which yields an f_{O_2} just below the iron-wüstite buffer.

Experimental products and analytical methods

The run products were analysed by X-ray diffraction, electron microprobe, and Mössbauer spectroscopy. The run conditions and the phases produced are listed in Table 1. The cell edges of the garnets were determined from the average of at least 10 peaks above 60° 2θ using Ge monochromated CoK_{α_1} radiation (STOE STADIP focussing diffractometer in transmission mode). Germanium or Si metal was used as an internal standard, with the Ge referenced to the NBS standard Si. Phase compositions were determined using a Cameca Camebax SX50 microprobe in wavelength dispersive mode using a 15 kV accelerating voltage and a 15 nA beam current. The standards were andradite for Ca, Fe_2O_3 for Fe, and either andradite or enstatite for Si. The raw counts were recalculated using the PAP correction scheme provided by Cameca. Garnet compositions were calculated assuming ideal stoichiometry of eight cations per formula unit and charge balance.

Resonant absorption spectra were collected at 298 K and 80 K with a Mössbauer spectrometer operating in constant acceleration mode and a $\approx$50 mCi ^{57}Co in Rh source. The velocity ramp was $\pm$ 5 mm/s. Mirror-image spectra were collected over 512 channels and calibrated with respect to α-Fe metal at room temperature. The samples were prepared so that the Fe concentration was <5 mg/cm^2 to avoid effects from saturation. The spectra were fit using the PC-MOS software obtained from CMTE Elektronik, Auenstraße 15, D-85521 Riemerling, Germany. Uncertainties in the obtained hyperfine parameters and area ratios are estimated to be $\pm$0.01 mm/s and $\pm$0.01 respectively.

Results and discussion

Garnet solid solutions

All garnets produced in this study are isotropic under oils. They are light yellow-brown at andradite-rich ($X_{and} > 0.70$) compositions and become progressively darker and redder with increasing skiagite content. None of the garnets are magnetic. The run conditions and product phases of each experiment are given in Table 1. The grain size is variable, but in some runs reached up to 200 μm, which permitted single crystal structural refinements to be made on five of the samples across the join. Results of the refinements and their crystal chemical implications are described in Woodland and Ross (1994).

The mole fraction of andradite was determined from the Ca content measured by the electron microprobe. The Fe^{2+} and Fe^{3+} contents were computed assuming ideal stoichiometry of 8 cations per formula unit and charge balance with 12 oxygens. In order to verify that Fe^{3+} and Fe^{2+} resided uniquely on the octahedral and dodecahedral sites respectively, a prerequisite for garnets to lie on the andradite-skiagite join, Mössbauer spectra were obtained on as many samples as possible. Details of the Mössbauer results are presented in Woodland and Ross (1994) and are only briefly summarised here. End-member andradite samples have a single doublet with a centre shift (CS) of 0.40 mm/s and quadrupole splitting (QS) of 0.55 mm/s at room temperature, which is in perfect agreement with literature values for andradite (Amthauer et al. 1976; Schwartz et al. 1980; Geiger et al. 1990). This doublet can be assigned as octahedrally coordinated Fe^{3+}. All spectra from the solid solutions and the skiagite end-member have two distinct doublets. One doublet has hyperfine parameters similar to those found for andradite and can also be attributed to Fe^{3+}. The other doublet, which grows in relative intensity with increasing skiagite content, has a much larger room temperature CS and QS of $\approx$1.3 mm/sec and $\approx$3.5 mm/s respectively. Comparison with results for almandine indicates that this doublet corresponds to dodecahedral Fe^{2+} (e.g. Amthauer et al. 1976; Woodland and O'Neill, 1993; Woodland and Ross 1994). No other Fe species are observable, confirming that the garnets are true binary compositions.

Unit cell parameters determined for the andradite - skiagite solid solutions are only slightly nonlinear with respect to composition (Table 1, Woodland and Ross 1994). A quadratic fit to the unit cell data gives: $a_o(\text{Å}) = 12.061(1) - 0.296(5)X_{ski} - 0.393(5)X_{ski}^2$ (Woodland and Ross, 1994). Our andradite, synthesised at 1100° C and 2.8 GPa has a unit cell parameter of 12.0596(2) Å, in excellent agreement with the results of Huckenholz and Yoder (1971) obtained between 0.1 and 3.0 GPa. The andradite synthesised from a glass in the presence of PtO_2 had a somewhat larger unit cell parameter due to the incorporation of $\approx$1 wt% Pt in the garnet (Woodland and Ross 1994). When Huckenholz and Yoder (1971) and Suwa et al. (1976) synthesised andradite at 1 bar in air near its high temperature stability limit ($\approx$1150° C), they obtained smaller unit cell parameters compared with andradites

Table 1 Experimental results; (*sk* skiagite, *gt* garnet, *cpx* clinopyroxene, *hd*, hedenbergite, *sp* spinel, *mt* magnetite, *hm* hematite, *q* quartz, *coe* coesite)

Experiment	*T* °C	*P* GPa	Time h	Intended composition	Phases produced	Gt composition probe	Cpx composition probe	Cell edge (Å) Gt	Sp	Sp Composition probe
An23	1300	1.4	4	Sk00	Gt			12.0690(5)		
Aw63[a]	1100	2.8	91	Sk00	Gt	Sk00		12.0596(2)		
Aw39a	1080	2.8	72.5	Sk10	Gt+(hm+q)[c]	Sk06		12.0457(15)		
Aw54a	1080	2.5	93	Sk10	Gt	Sk07		12.0375(4)		
Aw48[b]	1100	1.7	116.5	Sk20	Gt+sp+cpx+q	Sk12	Hd99.3	12.0255(8)		Mt96.5
Aw39b	1080	2.8	72.5	Sk20	Gt+sp+cpx	Sk18	Hd97.4	12.0045(6)		
Aw40	1080	3.5	72	Sk20	Gt+sp+cpx	Sk25	Hd91.4	11.9807(7)	8.389(1)	Mt94.7
Aw46	1000	1.6	24	Sk20	Gt+sp+cpx	Sk17	Hd97.1	12.0161(7)	8.395(1)	Mt97.8
Aw52a	1100	4.1	96.5	Sk20	Gt+(coe+cpx?)	Sk28		11.9755(1)		
Aw58[b]	1080	1.0	32	Sk20	Gt+sp+cpx	Sk06	Hd100	12.0386(5)	8.3937(8)	Mt98.3
Aw54b	1100	2.5	93	Sk20	Gt+cpx+sp	Sk08	Hd100	12.0361(7)	8.3882(4)	Mt93.7
Aw98a[b]	1100	2.4	72	Sk20	Gt	Sk18		12.0102(6)		Mt98
Aw98b[b]	1100	2.4	72	Sk20	Gt+q+sp+cpx	Sk18	Hd94.7	12.0040(5)	8.3945(10)	Mt98
Aw98c[b]	1100	2.4	72	Sk20	Gt+sp+cpx	Sk16	Hd95.8	12.0104(4)		Mt98
Aw41	1100	3.9	89.5	Sk30	Gt+sp+cpx	Sk27	Hd89.7	11.9803(8)	8.3906(11)	Mt94.2
Aw47	1100	4.8	46	Sk30	Gt+(cpx)	Sk36		11.9503(8)		
Aw52b	1100	4.1	96.5	Sk30	Gt+cpx+sp+coe	Sk34		11.9565(7)	8.389(1)	Mt93.6
Aw66	1080	2.5	120	Sk30	Gt+cpx+sp+q	Sk17		12.0153(6)	8.3912(4)	
Aw52c	1100	4.1	96.5	Sk40	Gt+sp+cpx+coe	Sk33	Hd84.9	11.9572(5)	8.3883(6)	Mt93.1
Uhp769	1100	5.4	12.5	Sk40	Gt+sp+cpx+coe	Sk40	Hd78	11.9382(3)	8.387(2)	Mt91.1
Uhp751a	1100	8.0	12.5	Sk50	Gt+sp+coe	Sk53		11.8911(6)		
Uhp697	1100	7.0	12.5	Sk50	Gt+(cpx+coe)	Sk55	Hd48.4	11.8880(5)		
Uhp659a	1100	6.0	12.5	Sk50	Gt+sp+coe+cpx	Sk48	Hd67.5	11.9150(7)	8.380(1)	
Uhp684a	1100	7.5	12.5	Sk60	Gt+coe+sp	Sk64		11.8580(5)		
Uhp654a	1100	7.0	12.5	Sk60	Gt+(sp+coe)	Sk63		11.8612(6)		
Uhp659b	1100	6.0	12.5	Sk60	Gt+sp+coe+cpx	Sk47	Hd66.7	11.9150(5)		
Uhp839a	1100	7.5	12.5	Sk70	Gt+sp+coe	Sk64		11.8559(8)	8.375(2)	
Uhp751b	1100	8.0	12.5	Sk70	Gt+coe+sp	Sk64		11.8541(7)		
Uhp684b	1100	7.5	12.5	Sk70	Gt+coe+sp	Sk64		11.8546(4)	8.3695(5)	
Uhp610	1100	8.5	12	Sk80	Gt+cpx+coe+sp(d)?	Sk78	Hd03	11.8025(6)		Mt37
Uhp654b	1100	7.0	12.5	Sk80	Gt+coe+sp+cpx	Sk64	Hd04.4	11.8568(7)	8.366(1)	Mt69.5
Uhp666	1100	9.3	12.5	Sk80	Gt	Sk79		11.8002(5)		
Uhp714a	1100	8.5	12.5	Sk80	Gt+coe+sp(d)?	Sk74		11.8204(6)		Mt75
Uhp839b	1100	7.5	12.5	Sk80	Gt+coe+sp	Sk70		11.8363(3)		
Uhp714b	1100	8.5	12.5	Sk90	Gt+coe+sp	Sk80		11.7923(9)	8.3431(4)	Mt65
Uhp755	1100	9.0	12.5	Sk90	Gt+(coe+sp(d)?)	Sk89		11.7683(7)		Mt57
Uhp825	1100	8.5	12.5	Sk90	Gt+sp+cpx+coe	Sk83	Hd01.9	11.7856(6)		Mt39.9
Uhp739	1100	9.7	12.5	Sk90	Gt+(sp+coe)	Sk89		11.7663(2)		
					Re-equilibration expts.					
Aw69r	1100	4.1	115	Sk12	Gt+cpx+sp+coe	Sk15				
Uhp835r	1100	6.0	14.5	Sk33	Gt+cpx+sp+coe	Sk44				Mt87
Uhp828r	1100	4.5	14.5	Sk40	2Gts+cpx+sp+coe	Sk33	Hd87.3			Mt96
Uhp769r	1100	5.4	12.5	Sk53	2Gts+sp+cpx+coe	Sk41	Hd74.1	11.9290(9)	8.385(2)	Mt91.4
Uhp697r	1100	7.0	12.5	Sk79	Gt+cpx+opx+spd+coe	Sk60		11.8681(17)		Mt48.5
Uhp765r	1100	8.0	12.5	Sk89	2Gts+coe+sp	Sk83		11.7990(9)		Mt66

[a] oxide mix
[b] used gold capsule
[c] trace phases in brackets

synthesised at lower temperatures; 12.051 Å and 12.045(2) Å compared to 12.059 Å and 12.057 Å from Suwa et al. (1976) and Huckenholz and Yoder (1971) respectively. This decrease is likely due to the presence of a small amount of Fe^{2+} and would correspond to ≈3–5 mol% skiagite based upon the unit cell parameter - composition relation given above. The maximum solubility of skiagite in andradite at 1 bar is currently unknown. Analysis of the derived molar volumes of the andradite - skiagite solid solutions indicates a small positive deviation from ideal behaviour with $W_v = 1.0 \pm 0.2\ cm^3\ mol^{-1}$ (Woodland and Ross 1994).

Phase relations

The maximum extent of Fe^{2+} substitution in andradite increases with increasing pressure (Table 1). This can easily be visualised in an isothermal section of a pressure - composition phase diagram (Fig. 1). The solubility of skiagite in andradite increases from 12 mol% at 1.7 GPa to 48 and 64 mol% at 6.0 and 7.0 GPa respectively (Table 1, Fig. 1). These values are greater than that found for the solubility of skiagite in almandine at the same pressure and temperature conditions (Woodland and O'Neill 1993). The trend of our results here, in the $CaO–FeO–Fe_2O_3–SiO_2$ system, is consistent with end-member skiagite becoming stable at ≈9.3 GPa and 1100° C, as reported by Woodland and O'Neill (1993). A multi-phase assemblage appears when the bulk composition of the starting material differs from the stable garnet composition at a given pressure. Andradite is stable at 1100° C and 1 bar in air and breaks down to pseudowollastonite and hematite at 1137–1165° C (Huckenholz and Yoder 1971; Suwa et al. 1976). The phase relations in the Fe^{2+}-bearing

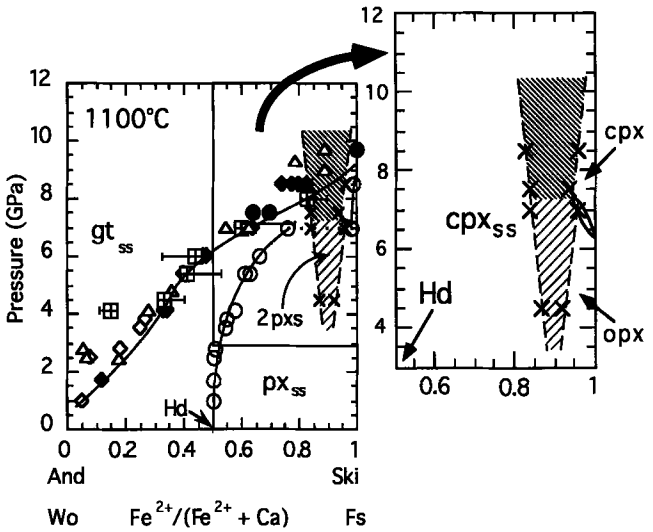

Fig. 1 Phase relations for andradite - skiagite garnet and hedenbergite–ferrosilite pyroxene solid solutions as a function of pressure up to 12.0 GPa at 1100° C. The coexisting clinopyroxene compositions, defining part of the divariant loop are represented by the *open circles*. *Open triangles* are garnet ± traces of other phases; *open diamonds* are garnet + spinel + clinopyroxene; *closed diamonds* are garnet + spinel + SiO_2 + clinopyroxene; *closed circles* are garnet + spinel + SiO_2; *crossed squares* are the re-equilibration experiments with the approach to equilibrium shown; the *xs* represent the coexisting pyroxene compositions that define the miscibility gap. The *coarse cross-hatched* region at lower pressures indicates miscibility between hedenbergite s.s. and Ca-poor orthopyroxene; the *finer cross-hatching* demarcates the miscibility gap between two clinopyroxenes. A small binary loop is present between the Ca-poor orthopyroxene and the Ca-poor high pressure clinopyroxene

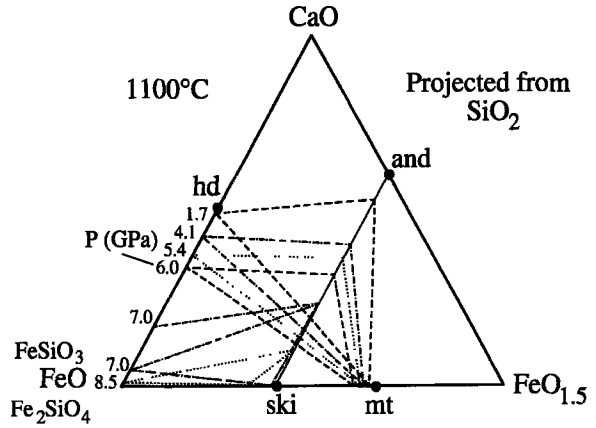

Fig. 2 Plot of the system CaO–FeO–$FeO_{1.5}$ projected from SiO_2 showing phase assemblages as a function of pressure at 1100° C. Pyroxene and spinel solid solutions plot along the *left* side and *base* of the diagram respectively. Coexisting garnets plot along the *line* between andradite (*and*) and skiagite (*ski*). For clarity, the tie-lines linking the coexisting phases at different pressures are shown in *different patterns*. The intersection of the pyroxene miscibility gap is depicted in the assemblage at 7.0 GPa. Note the shift in spinel composition with increasing pressure

system are complicated at low pressure by the presence of ferrobustamite, a pyroxenoid, and it is not until ≈0.7 GPa that hedenbergite ($CaFeSi_2O_6$) becomes stable at 1100° C (Lindsley 1967). Above 0.7 GPa, the maximum skiagite solubility is governed by the equilibrium:

$$Fe_3^{2+}Fe_2^{3+}Si_3O_{12} = Fe_3O_4 + Fe_2Si_2O_6 + SiO_2 \quad (3)$$

garnet spinel clinopyroxene quartz/coesite

The $Fe_2Si_2O_6$ component in the clinopyroxene increases with increasing pressure and skiagite content, defining with the garnet a divariant loop in pressure - composition space (Fig. 1). The extensive solid solution between hedenbergite ($CaFeSi_2O_6$) and ferrosilite ($Fe_2Si_2O_6$) stabilises pyroxene as a coexisting phase to higher pressures than are observed with almandine–skiagite garnets, where the coexisting pyroxene is essentially pure ferrosilite (Woodland and O'Neill 1993). The coexisting spinel is magnetite-rich, although there is an increase in the Fe_2SiO_4 component with increasing pressure and skiagite content. For example at 6.0 GPa, the spinel has a composition of 13 mol% Fe_2SiO_4 and 87 mol% Fe_3O_4 (experiment uhp835r in Table 1). This is apparent in the plot of the CaO–FeO–$FeO_{1.5}$ composition space projected from SiO_2 in Fig. 2. In several experiments with andradite-rich compositions, quartz or coesite was absent (Table 1). It is not clear why this occurred since quartz was present in experiments at similar conditions using the same starting glass (aw98b and aw40, for example, see Table 1).

Above ≈7.0 GPa, there are two stable assemblages involving andradite–skiagite solid solutions depending on the starting bulk composition. For compositions on the Fe^{3+}-rich, or oxidising side of the andradite–skiagite join, clinopyroxene becomes unstable relative to spinel + coesite. In this case, the garnet composition is controlled by the equilibrium between garnet, spinel and coesite:

$$Fe_3^{2+}Fe_2^{3+}Si_3O_{12} = Fe_3O_4 + Fe_2SiO_4 + 2SiO_2 \quad (4)$$

garnet spinel spinel coesite

This is the low pressure terminal reaction for pure skiagite in the FeO–Fe_2O_3–SiO_2 subsystem, which occurs at about 9.3 GPa at 1100° C (Woodland and O'Neill 1993).

For bulk compositions on the Fe^{2+}-rich, or reduced side of the andradite–skiagite join, clinopyroxene remains stable and reaction (3) continues to define the maximum skiagite content in the garnet. At these relatively high pressures, the clinopyroxene has a composition close to the ferrosilite end-member due to the intersection of the pyroxene miscibility gap with the divariant loop (Fig. 2 and see below). This causes the deflection in the divariant loop shown in Fig. 1. Nevertheless, the small amount of Ca substitution in the pyroxene is apparently sufficient to stablise this phase relative to Si-rich spinel + coesite,

the assemblage which is observed in equilibrium with almandine–skiagite solid solutions in the same pressure range (Woodland and O'Neill 1993). In one case at 7.0 GPa, (experiment uhp697r) a spinelloid with a composition of 48.5 mol% Fe_2SiO_4 and 51.5 mol% Fe_3O_4 was present rather than a true spinel (identified by XRD). This is consistent with the results of Ross et al. (1992), who reported a spinelloid phase at intermediate compositions along the Fe_2SiO_4–Fe_3O_4 join at 7.0 GPa. For a couple of other experiments at 8.0 and 8.5 GPa, the combination of peak overlap with coexisting phases and low peak intensities precluded the determination of whether a spinel or a spinelloid was present. However, spinel was positively identified in experiment uhp825 at 8.5 GPa, which was Fe_2SiO_4-rich with a $Fe^{3+}/\Sigma Fe$ ratio less than that of the coexisting garnet (Fig. 2).

Reversals

In addition to the synthesis experiments, six experiments were performed with previously synthesised garnet or garnet-bearing mixtures in an attempt to reverse the garnet composition (Table 1, Fig. 1). In four experiments, the garnet was re-equilibrated at a lower pressure than the original synthesis pressure. Under these conditions, a new garnet formed that was richer in andradite than the original garnet. These experiments, therefore, approached equilibrium from the direction of high Fe^{2+} (skiagite) content in the garnet. As is apparent in Fig. 1, the results of these experiments are in very good agreement with those of the synthesis experiments. A small amount of Al contamination was detected in sample uhp697r during microprobe analysis. The contamination presumably occurred either during extraction of the garnet sample that was synthesised at high pressure and subsequently used in the re-equilibration experiment, or during loading of the capsule. Aluminum was detected only in the garnet, 0.020 cations pfu (per formula unit), indicating a strong partitioning of Al into garnet over the coexisting clinopyroxene or spinelloid. This strong preference of Al for garnet is also observed between almandine–skiagite garnet solid solutions and coexisting orthopyroxene and spinel (Woodland and O'Neill 1993). Two pyroxenes with different compositions are present coexisting with the Al-bearing garnet in uhp697r (see below).

The approach to equilibrium from the direction of high Ca (andradite) content was evaluated in two experiments. In experiment aw69, an aliquot from experiment aw48 containing garnet (ski12), clinopyroxene, spinel, and quartz was re-equilibrated at a pressure of 4.1 GPa. The garnets had rim compositions slightly richer in Fe^{2+}, up to ski15. Another experiment, uhp835r, employed a mixture from aw52c of ski33, clinopyroxene, spinel, and coesite along with enough ferrosilite and hematite to increase the nominal skiagite content to 53 mol%. Heterogeneous garnets resulted and the rim composition with the highest skiagite content (ski44) was taken to be closest to the equilibrium value (Table 1, Fig. 1).

Spinel

The coexisting spinels were fine grained, almost always ≤ 10 μm across. In a number of samples, the spinels were too fine grained to permit microprobe analysis. Structural formulae were computed from the microprobe analyses assuming ideal R_3O_4 stoichiometry and charge balance. The mole fraction of Fe_2SiO_4 was obtained directly from the Si content. Although a small amount of Ca, generally <0.5 wt% CaO (corresponding to ≤ 2 mol% of a $CaFe_2O_4$ component), was detected in all samples, it is difficult to be sure how much of this was due to fluorescence from the adjacent Ca-rich garnet or pyroxene grains. Accordingly, the Ca was ignored in computing the structural formulae and the spinels were assumed to be strictly binary Fe_3O_4–Fe_2SiO_4 solid solutions. Fluorescence is a particular problem because of the fine grained nature of the spinels (cf. Köhler and Brey 1990).

Like the spinel coexisting with almandine–skiagite solid solutions (Woodland and O'Neill 1993), the $X_{Fe_2SiO_4}$ increases with increasing pressure and skiagite content in the garnet (Table 1, Fig. 2). The occurrence of a spinelloid rather than a spinel in at least one experiment (uhp697r) further emphasises the fact that there is considerable complexity of the phase relations, even in the essentially three component FeO–Fe_2O_3–SiO_2 system at high pressures (see also Ross et al. 1992). This is in contrast to the simplicity of the system at atmospheric pressure, where only two binary phases (Fe_2SiO_4 olivine and Fe_3O_4 spinel) and no ternary phases are stable.

Pyroxenes

Pyroxene coexisting with andradite–skiagite solid solutions changes composition as a function of pressure and bulk composition (Table 1, Fig. 1). At pressures below ≈ 3.0 GPa, the pyroxene is close to pure hedenbergite with only minor ferrosilite substitution, ≤ 5 mol% (Table 1, Fig. 1). Above ≈ 3.0 GPa, the ferrosilite content steadily increases with increasing pressure until 7.0 GPa, where there is a discontinuous shift to very ferrosilite rich compositions, >95 mol% $Fe_2Si_2O_6$. This discontinuity, along with the occurrence of two pyroxenes in the reversal experiment uhp697r, indicates the presence of a miscibility gap in $CaFeSi_2O_6$–$Fe_2Si_2O_6$ pyroxenes at 7.0 GPa and 1100° C (Table 1, Fig. 1). Comparison with results for the FeO–Fe_2O_3–SiO_2 subsystem (Woodland and

Table 2 Results of experiments that define the pyroxene miscibility gap

Experiment	T °C	P GPa	Time h	Starting composition	Final composition Clinopyroxene	Orthopyroxene
Uhp828p	1100	4.5	14.5	Hd20	Hd26	Hd17
Uhp697r[a]	1100	7.0	12.5	Sk79	Hd32	Hd07.4
Uhp781p	1100	7.5	12.5	Hd20	Hd35, hd13	
Uhp825p	1100	8.5	12.5	Hd20	Hd34, hd10	

[a] Oxide mix

O'Neill 1993) indicates that pyroxene must become unstable relative to Si-rich spinel + coesite between 8.5 and 9.3 GPa at 1100° C.

An additional complexity is that the Ca-poor pyroxene undergoes a structural transition from orthorhombic orthoferrosilite (space group Pbca) to a high pressure monoclinic phase. This transition occurs between 7.0 and 7.5 GPa at 1100° C, based upon the results of experiments Uhp697r and Uhp781p (Table 2). The X-ray diffraction pattern of the monoclinic phase was indexed in the $P2_1/c$ space group. However, Hugh-Jones et al. (1994) has demonstrated that end-member clinoferrosilite with the $P2_1/c$ structure transforms to an unquenchable high pressure polymorph having the C2/c space group between 1.5 and 1.8 GPa at room temperature. A similar transition has been observed in $Mg_2Si_2O_6$ (Angel et al. 1992). It is likely that the Ca-poor clinopyroxene in our experiments above $\approx$7.0 GPa at 1100° C also had this high pressure C2/c structure and subsequently transformed to $P2_1/c$ during the quench.

There is in fact more than one distinct C2/c polymorph of $Fe_2Si_2O_6$ (Hugh-Jones et al. 1994). A low-pressure form was obtained by Sueno et al. (1984) by heating orthoferrosilite at atmospheric pressure. It is metastable with respect to Fe_2SiO_4 (olivine) + SiO_2 (quartz). A third polymorph can be postulated as a fictive $Fe_2Si_2O_6$ end-member, having a hedenbergite-like structure that would form the Fe-rich end-member of the $CaFeSi_2O_6$–$Fe_2Si_2O_6$ solid solutions studied by Lindsley and Munoz (1969) and Lindsley (1980, 1981). The structure of this 'fictive' end-member can be approximated by extrapolating the data for the hedenbergite-clinoferrosilite solid solutions of Cameron et al. (1973) and Ohashi et al. (1975). The resulting structure is similar to that of the low pressure polymorph of Sueno et al. (1984), having a relatively large M2 site with 8-fold coordination, suggesting that these two polymorphs are one and the same (Hugh-Jones et al. 1994). For simplicity, we will refer to the low-pressure C2/c monoclinic pyroxene solid solution series as "hedenbergite s.s.". In contrast, the high pressure form of C2/c clinoferrosilite encountered in this study has a markedly different structure with a much smaller, 6-fold coordinated, and highly distorted M2 site, somewhat similar to that in orthoferrosilite (Hugh-Jones et al. 1994).

Immiscibility in $CaFeSi_2O_6$–$Fe_2Si_2O_6$ clinopyroxenes

In order to define better the miscibility gap in Ca-Fe pyroxenes, three additional experiments were performed with bulk compositions on the $CaFeSi_2O_6$–$Fe_2Si_2O_6$ join. Guided by the results from experiment uhp697r and the lower pressure and temperature experiments of Lindsley and Munoz (1969) and Lindsley (1980), the starting composition was 80 mol% $Fe_2Si_2O_6$-20 mol% $CaFeSi_2O_6$, prepared from a mixture of ferrosilite and wollastonite. Two pyroxenes were observed in the X-ray diffraction pattern and backscattered images from each of the experiments, with the analysed compositions taken to define the extent of the miscibility gap (Table 2, Fig. 1). At pressures of $\approx$7.0 GPa and lower, the compositional extent of the hedenbergite s.s. is constrained by its coexistence with Ca-poor *ortho*pyroxene solid solutions. The compositions of these coexisting solid solutions have been determined at 4.5 and 7.0 GPa (Table 2). At $\geq$7.5 GPa, the composition of the hedenbergite s.s. is terminated by its coexistence with high-pressure Ca-poor *clino*pyroxene solid solutions. We have determined the extent of this miscibility gap at 7.5 and 8.5 GPa (Table 2, Fig. 1). The form of the miscibility gap as a function of temperature awaits further experiments.

We have retained the general term "miscibility" gap rather than "solvus" to refer to the compositional gap between the hedenbergite s.s. and the high pressure Ca-poor clinopyroxene phase. The term "solvus" is usually restricted to a system in which the free energy of mixing in the solid solution is a continuous function of composition. This implies that the two end-members have the same crystal structure, so that there are no structural discontinuities in passing from one to the other. Such is clearly the case for the hedenbergite s.s., which, at high temperatures and low pressures, might reasonably be inferred to change smoothly and continuously between the hedenbergite and low pressure C2/c clinoferrosilite end-members, were the latter thermodynamically stable (i.e. with respect to orthoferrosilite

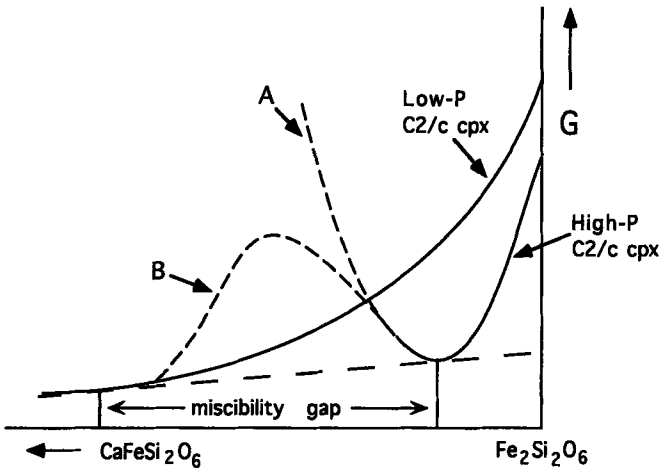

Fig. 3 Schematic diagram of the *G–X* curves for C2/c hedenbergite–clinoferrosilite solid solutions, drawn at a temperature and pressure where the high pressure polymorph is stable. The very asymmetric miscibility gap between the high pressure form and the low pressure solid solution is represented. We have indicated two possibilities for the form of the *G-X* curve for the high pressure solid solution. Curve A is independent of the *G-X* curve for the low pressure solid solution, as is usually the case for a first-order transition between two polymorphs. However, since the two polymorphs have the same space group, it is possible to imagine a continuous change from the low pressure to the high pressure forms with changing composition. This possibility is indicated by curve *B*

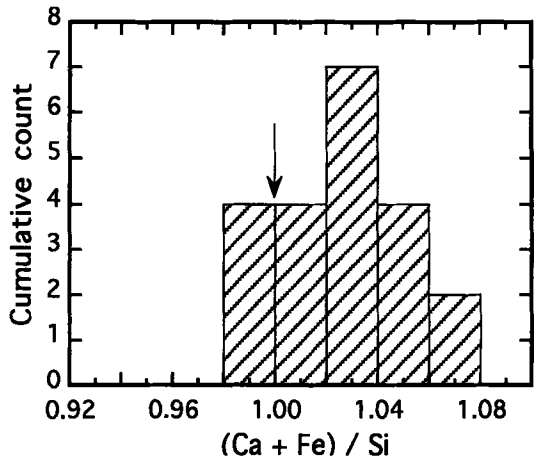

Fig. 4 Histogram of (Ca + Fe)/Si in hedenbergite solid solutions from 21 experiments. Ratios of 1.0, denoted by the *arrow*, are for stoichiometric $CaFeSi_2O_6$–$Fe_2Si_2O_6$ pyroxenes. Values > 1.0 imply the presence of Fe^{3+} as a ferri-Tschermak's component

or fayalite plus quartz). Although the high pressure Ca-poor clinopyroxene solid solutions have the same space group as the hedenbergite s.s., their detailed structure is sufficiently dissimilar to throw doubt on whether a continuous transition between the two can occur: hence our use of the general term miscibility gap. If such a continuous transition could occur, then it would lead to a branching in the free energy-composition curve, illustrated schematically by curve 'B' in Fig. 3. This is an unusual situation and we are unaware of any analogous systems exhibiting such a phenomenon. Note also that there are relatively large differences in the molar volume of the low and high pressure C2/c clinoferrosilite polymorphs. This might lead to some additional complexity at higher pressures, with the high pressure structure extending its stability field to the Ca-rich side of the miscibility gap.

The highly asymmetric geometry of the miscibility gap between the hedenbergite s.s. and the high pressure C2/c low Ca pyroxene contrasts with the nearly symmetric miscibility gap (solvus) developed by the hedenbergite s.s. below 860° C at 2.0 GPa (Lindsley and Munoz 1969). This contrasting behaviour can be understood on purely structural grounds by comparison of the structures of the low and high pressure clinoferrosilite polymorphs. As noted above, the M2 site in high pressure C2/c clinoferrosilite is relatively small, rather like that of orthoferrosilite (Hugh-Jones et al. 1994). It might be expected that this smaller site would not be as amenable to substitution by a large cation like Ca. In fact, in $CaMgSi_2O_6$-$Mg_2Si_2O_6$ pyroxenes, the analogous high pressure C2/c clinoenstatite phase is calculated to contain slightly less Ca than coexisting orthoenstatite in equilibrium with diopside solid solution (Gasparik 1990; see his Fig. 2n). Therefore, the Ca content of high pressure C2/c pyroxene in equilibrium with a hedenbergite s.s. may also be expected to be low, like that in orthoferrosilite. This is supported by the results illustrated in Fig. 1, where there is no significant discontinuity in the miscibility gap when passing into the C2/c stability field with increasing pressure.

Fe^{3+} in pyroxenes

The possible presence of Fe^{3+} as the ferri-Tschermak's ($CaFe^{3+}_2SiO_6$) component adds potential complexity to the pyroxene composition. Since pyroxenes always occurred in multi-phase assemblages in our experiments, direct measurement of Fe^{3+} by Mössbauer spectroscopy was not possible. However, an assessment of the Fe^{3+} content can be made from the cation ratio (Ca + Fe)/Si determined from the microprobe analyses. When this ratio differs from 1.0, a deviation in composition from the stoichiometric $CaFeSi_2O_6$–$Fe_2Si_2O_6$ binary is indicated. A ratio greater than 1.0 can be attributed to the $CaFe^{3+}_2SiO_6$ substitution. The (Ca + Fe)/Si ratio is shown for pyroxenes from 21 samples in Fig. 4. Eight samples have (Ca + Fe)/Si $\approx 1.0 \pm 0.02$ (the likely uncertainty in the analyses), but the remaining 13 samples have cation ratios slightly greater than 1.0, up to a maximum of 1.07. Therefore, the Fe^{3+} content in the clinopyroxene is small, corresponding to a maximum of 3.5 mol% $CaFe^{3+}_2SiO_6$. This indicates that Fe^{3+} is strongly partitioned into the coexisting spinel and garnet. Although the maximum ferri-Tschermak's substitution in hedenbergite is presently unknown, Huckenholz et al. (1969) found up to 28

mol% of this component could substitute into diopside at 1175° C and 1 bar. Our relatively low Fe^{3+} contents may be due to the fact that the clinopyroxenes are in equilibrium with spinel rather than hematite as in the experiments of Huckenholz et al. (1969).

Ca–Fe^{2+} partitioning between clinopyroxene and garnet

The distribution of Ca and Fe^{2+} between coexisting garnet and clinopyroxene can be considered through the exchange equilibrium:

$$\underset{\text{garnet}}{1/3Ca_3Fe_2^{3+}Si_3O_{12}} + \underset{\text{clinopyroxene}}{Fe_2^{2+}Si_2O_6} = \underset{\text{garnet}}{1/3Fe_3^{2+}Fe_2^{3+}Si_3O_{12}} + \underset{\text{clinopyroxene}}{CaFe^{2+}Si_2O_6} \quad (5)$$

The condition of equilibrium, with a standard state of the pure phases at the pressure and temperature of interest is:

$$\frac{-\Delta G^o}{RT} = \ln \frac{X^{gt}_{ski} X^{cpx}_{hd}}{X^{gt}_{and} X^{cpx}_{cfs}} + \ln \frac{\gamma^{gt}_{ski} \gamma^{cpx}_{hd}}{\gamma^{gt}_{and} \gamma^{cpx}_{cfs}} = \ln K_D + \ln K\gamma \quad (6)$$

In Eq. 6, activities have been replaced by mole fractions (X_i^j) and activity coefficients (γ_i^j) as follows:

$$a^{gt}_{Fe_3Fe_2Si_3O_{12}} = (X^{gt}_{Fe}\gamma^{gt}_{Fe})^3$$

$$a^{cpx}_{Fe_2Si_2O_6} = (X^{cpx}_{Fe}\gamma^{cpx}_{Fe})$$

with analogous substitutions for the Ca-bearing components. Values of ln K_D for reaction 5 is plotted in Fig. 5 as a function of $Fe_2Si_2O_6$ content in the clinopyroxene. The data shown are limited to those experiments in which the clinopyroxene had a composition on the Ca-rich side of the miscibility gap. This was done because the thermodynamic properties of the high pressure clinoferrosilite are as yet poorly constrained. The values of K_D in Fig. 5 are uncorrected for the effect of pressure. The pressure effect is small with ΔV_{298} (5) = −0.208 J/b, using the molar volumes of hedenbergite from Cameron et al. (1973), skiagite and andradite from this study, and of low pressure C2/c clinoferrosilite from Lindsley (1981), obtained by extrapolating the data for the hedenbergite solid solutions of Cameron et al. (1973) and Ohashi et al. (1975).

The mixing properties of the andradite–skiagite solid solutions can be derived from the K_D data if the properties of the Ca–Fe pyroxenes are known independently. Lindsley (1981) developed a model for hedenbergite solid solutions from the solvus in this join. This binary model was later incorporated into the more general model for quadrilateral pyroxenes of Davidson and Lindsley (1985). The appropriate expressions for the pyroxene activity coefficients are:

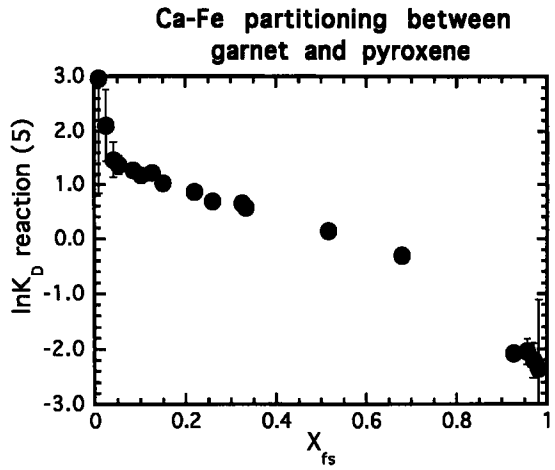

Fig. 5 Plot of ln K_D for reaction 5 as a function of ferrosilite content in pyroxene. The values are not corrected for the effect of pressure, which is small. The uncertainties are 1σ computed from the microprobe analysis of the coexisting garnet and pyroxene. Where error bars are not visible, the uncertainties are smaller than the size of the symbol (for both axes)

$$RT\ln\gamma_{hd} = X^2_{fs}[W_{hd} + 2(W_{fs} - W_{hd})X_{hd}]$$
$$RT\ln\gamma_{fs} = X^2_{hd}[W_{fs} + 2(W_{hd} - W_{fs})X_{fs}] \quad (7)$$

where W_{hd}(J/mol) = 20697 − 0.00235P (bar) and W_{fs}(J/mol) = 16941 + 0.0059P(bar) from Lindsley (1981). The small amounts of Fe^{3+} in our pyroxenes were ignored in this analysis.

Considering garnet as a symmetric solid solution, we have on a one gram-atom basis:

$$RT\ln\gamma_{and} = W_{gt}X^2_{ski}$$
$$RT\ln\gamma_{ski} = W_{gt}X^2_{and} \quad (8)$$

This is a reasonable assumption in view of the symmetric behaviour of the excess volumes of mixing across the andradite–skiagite join (Woodland and Ross 1994) and the limited number of data available (n = 12).

Substituting Eqs. 7 and 8 into Eq. 6 and simplifying gives:

$$RT\ln K_D + \int_1^P \Delta V_{298}(5)dP = -\Delta G^o_{T,1bar} + W_{gt}(2X_{ski} - 1) + (W_{hd})(2X_{fs} - 3X^2_{fs}) + (W_{fs})(1 - 4X_{fs} + 3X^2_{fs}) \quad (9)$$

With the assumption of $\int_1^P \Delta V_{298} = P\Delta V_{298}$, we obtained W_{gt} = −12.69(1.74)kJ/mol and $\Delta G^o_{1373K,1bar}$ = 13.14 (0.61) kJ/mol by weighted non-linear least squares regression of Eq. 9 (χ^2_ν = 1.33). Uncertainties of ±1 kbar (piston cylinder) or ±3 kbar (multi-anvil

press) and $\pm 5°$ C were assumed for the pressure and temperature of the experiments.

The large negative value for $W^{gt}_{Ca-Fe^{2+}}$ contrasts with results for mixing of Ca and Fe^{2+} on the analogous Al-garnet binary $Ca_3Al_2Si_3O_{12}$–$Fe_3Al_2Si_3O_{12}$ (grossular–almandine). Rather large positive deviations from ideality were proposed by Ganguly and Saxena (1984) and Anovitz and Essene (1987), however, more recent data of Koziol (1990) and Geiger et al. (1987) indicate small asymmetric deviations from ideality. Negative deviations from ideality are rare (perhaps unknown) in simple solid solution systems which do not involve order-disorder phenomena or other structural complications, and we regard this feature as throwing doubt on the present results. However, if confirmed, the large differences in the Ca-Fe^{2+} mixing properties between Al-garnets and Fe^{3+}-garnets would cause hitherto unforseen complications in modelling the activity - composition relations in compositionally complex natural garnet solid solutions.

The above value of $\Delta G^{o}_{1373K,1bar}$ for equilibrium (5) can be used to calculate $\Delta_f G^{o}_{1373K,1bar}$ for skiagite by combining it with thermodynamic data of Holland and Powell (1990) for andradite, hedenbergite, and orthoferrosilite. Since we are interested in the equilibrium involving the hedenbergite s.s., for which the Fe-rich end-member is low *P* clinoferrosilite, we used Holland and Powell's (1990) data for orthoferrosilite corrected by the ΔG for the transformation reaction:

$Fe_2Si_2O_6 = Fe_2Si_2O_6$

orthoferrosilite low P C2/c clinoferrosilite

for which Lindsley (1981) gives a value of $\Delta G = 1843$ J/mol. With these data, we obtain $\Delta_f G^{o}_{1373K,1bar} = -2939.89$ kJ/mol, which is 35.33 kJ/mol less negative than the value reported in Woodland and ONeill (1993).

This large discrepancy along with the unexpected large negative value of $W^{gt}_{Ca-Fe^{2+}}$ both point to a problem with our thermodynamic modelling of reaction (5). One possibility is the presence of Fe^{3+} in the pyroxene as a $CaFe^{3+}_2SiO_6$ component. However, the effect of such minor amounts of Fe^{3+} estimated to be in our pyroxenes (see above) could not account for such a large discrepancy. Another possibility could lie with the assumed formulation of the activity-composition model for the Ca–Fe pyroxenes. The model of Lindsley (1981) treats $CaFe^{2+}Si_2O_6$ (hedenbergite) as an end-member, which implies that as the composition of the solution approaches pure hedenbergite, the excess free energy of mixing of the solid solution approaches zero and the chemical potential of the $Fe_2Si_2O_6$ component must tend towards minus infinity. This is shown schematically as curves 'H' in Fig. 6a and b. An alternative is that $Fe_2Si_2O_6$ has a finite chemical potential at the $CaFeSi_2O_6$ composition implying that free energy varies continuously between the $Fe_2Si_2O_6$ and $Ca_2Si_2O_6$ components with an inflection occurring at the $CaFeSi_2O_6$ composition (curves 'C' in Fig. 6a and b). The difference in free energy between the two models at the hedenbergite composition is equal to the free energy of the reaction:

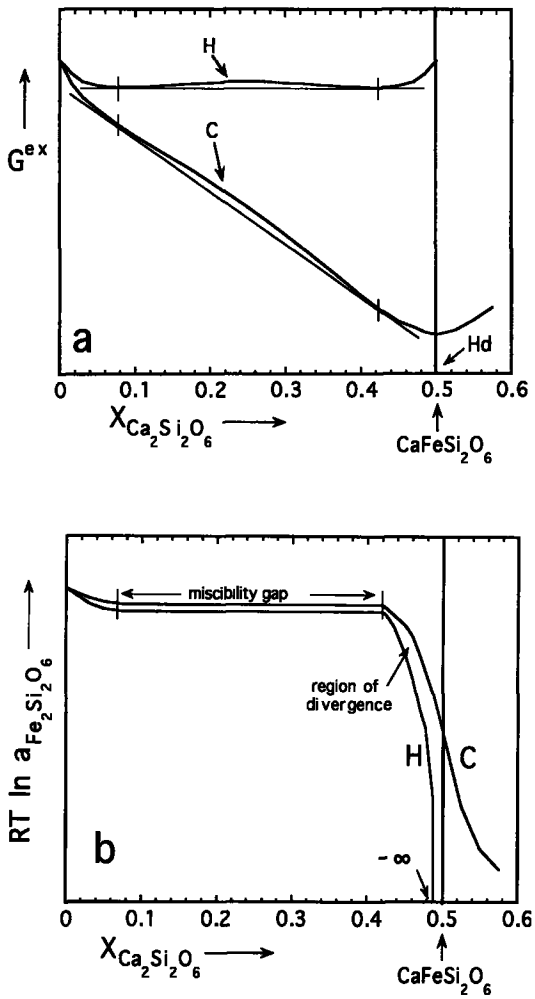

Fig. 6a, b Schematic G-*X* diagrams of part of the $Ca_2Si_2O_6$–$Fe_2Si_2O_6$ join drawn just below the miscibility temperature (the conditions of Lindsley's 1981 experiments) to illustrate the diverging behaviour near the hedenbergite composition depending on whether hedenbergite (*curves H*) or $Ca_2Si_2O_6$ (*curves C*) is considered as the Ca-rich clinopyroxene end-member. **a** Schematic G^{ex}-*X* diagram. Although both models can reproduce the identical miscibility gap, there is divergence near the hedenbergite composition where curve '*H*' must approach zero. **b** Schematic plot of *RT* ln $a_{Fe_2Si_2O_6}$ versus composition illustrating the divergence in the two models near the hedenbergite composition, even though both models are in close agreement over most of the join. When hedenbergite is the end-member, *RT* ln $a_{Fe_2Si_2O_6}$ must go to minus infinity at the hedenbergite composition. In contrast, finite values of *RT* ln $a_{Fe_2Si_2O_6}$ are obtained when $Ca_2Si_2O_6$ is considered as the Ca-rich end-member.

$0.5Fe_2Si_2O_6 + 0.5Ca_2Si_2O_6 = CaFeSi_2O_6$

This second possibility has been discussed in detail for the analogous $Mg_2Si_2O_6$–$CaMgSi_2O_6$ join by

Davidson et al. (1982). It is also similar to $CaFeSiO_4$–Fe_2SiO_4 olivine solid solutions, as recently discussed by P. Shi and H.St.C. O'Neill (in preparation), for which measurements of the activity of Fe_2SiO_4 have been made at compositions extending through the $CaFeSiO_4$ point and onto the $CaFeSiO_4$–Ca_2SiO_4 join (Johnson and Muan 1967). The $CaFeSiO_4$ composition is thus merely a point midway on the join between the Fe_2SiO_4 and Ca_2SiO_4 components, the latter being better chosen as end-members.

P. Shi and H.St.C. O'Neill (in preparation) provide two observations relevant to the present discussion of Ca–Fe clinopyroxenes. Firstly, they found that data defining the solvus could be satisfied equally well using either a simple model with Fe_2SiO_4 and $CaFeSiO_4$ as end-members or using an order - disorder model with Fe_2SiO_4 and Ca_2SiO_4 as end-members and a large range of $Ca\text{-}Fe^{2+}$ ordering energy. In fact, the former may be regarded as a special case of the latter where the ordering energy is infinite. Secondly, they found a large difference between the two models for the activity of Fe_2SiO_4 in the compositional range 20% Fe_2SiO_4-80% $CaFeSiO_4$ (or 60% Fe_2SiO_4-40% Ca_2SiO_4). Only the order-disorder model allowed them to fit both the solvus data and the available activity-composition data of Johnson and Muan (1967). The implication is that for solid solutions that contain a highly ordered phase at the midpoint composition, solvus data alone are not sufficient to determine activity-composition relations for compositions near to this midpoint composition.

The assessment of $Ca\text{-}Fe^{2+}$ partitioning between pyroxene and garnet in our experiments employed the clinopyroxene solution model of Lindsley (1981). However, Lindsley's (1981) model is based solely upon the determination of the solvus and, therefore, his model is not capable of deriving $Fe_2Si_2O_6$ activities near the hedenbergite composition. The large differences between Lindsley's (1981) model and an order-disorder model which takes $Ca_2Si_2O_6$ as an end-member can be appreciated by comparing the schematic $RT\ln a_{Fe_2Si_2O_6}$ versus composition curves 'H' and 'C' in Fig. 6b. Over most of the compositional range, the two curves are very similar, and therefore, the solvus is reproduced equally well by both models. However, as one approaches the hedenbergite composition, the two curves sharply diverge yielding large differences in $a_{Fe_2Si_2O_6}$. Unfortunately, 8 of the 12 data used in our regression fall within the problematic compositional range of $X_{hd} \geq 0.8$. We suggest that the discrepancy between our present attempt at determining $\Delta_f G^0_{1373K,1bar}$ of skiagite from reaction (5) and our previous value (Woodland and O'Neill 1993) is primarily caused by the inadequacy of the hedenbergite s.s. model in this compositional range. Confirmation of this proposal must await new data on the thermodynamic properties of the hedenbergite s.s. We note that the experiments of Gudmundsson and Wood (1995) do support our previous value for $\Delta_f G^o_{1373K,1bar}$ of skiagite.

Acknowledgements This project was initiated during the tenure of a fellowship from the Alexander von Humboldt Stiftung to ABW. H. Schulze is gratefully acknowledged for his expert help in sample preparation. D. Canil, C. McCammon, C. Ross II, and F. Seifert are thanked for their help and stimulating discussions during the course of the project. The manuscript benifited from the review of H. Huchkenholz.

References

Amthauer G, Annersten H, Hafner SS (1976) The Mössbauer spectrum of ^{57}Fe in silicate garnets. Zeit Kristallogr 143:14–55

Angel RJ, Chopelas A, Ross NL (1992) Stability of high-density clinoenstatite at upper mantle pressures. Nature 358:322–324

Anovitz LM, Essene EJ (1987) Compatibility of geobarometers in the system CaO–FeO–Al_2O_3–SiO_2–TiO_2 (CFAST):implications for garnet mixing models. J Geol 95:633–645

Cameron M, Sueno S, Prewitt CW, Papike JJ (1973) High-temperature crystal chemistry of acmite, diopside, hedenbergite, jadite, spodumene, and ureyite. Am Mineral 58:594–618.

Chou I-M (1986) Permeability of precious metals to hydrogen at 2 kbar total pressure and elevated temperatures. Am J Sci 286:638–658

Davidson PM, Lindsley DH (1985) Thermodynamic analysis of quadrilateral pyroxenes. II. Model calibration from experiments and application to geothermometry. Contrib Mineral Petrol 91:390–404

Davidson PM, Grover J, Lindsley DH (1982) $(Ca,Mg)_2Si_2O_6$ clinopyroxenes:a solution model based on nonconvergent site-disorder. Contrib Mineral Petrol 80:88–102

Ganguly J, Saxena SK (1984) Mixing properties of aluminosilicate garnet:constraints from natural and experimental data, and application to geothermo-barometry. Am Mineral 69:88–97

Gasparik T (1990) A thermodynamic model for the enstatite-diopside join. Am Mineral 75:1080–1091

Geiger CA, Newton RC, Kleppa OJ (1987) Enthalpy of mixing of synthetic almandine-grossular and almandine-pyrope garnets from high temperature solution calorimetry. Geochim Cosmochim Acta 51:1755–1763.

Geiger CA, Merwin L, Sebald A (1990) Ordering studies in grossular and pyrope garnets using ^{29}Si NMR and ^{57}Fe Mössbauer spectroscopy. Terra Abstr 2:75

Gudmundsson G, Wood BJ (1995) Experimental tests of garnet peridotite oxygen barometry. Contrib Mineral Petrol 119:56–67

Gustafson WI (1974) The stability of andradite, hedenbergite, and related minerals in the system Ca–Fe–Si–O–H. J. Petrol 15:455–496

Holland TJB, Powell R (1990) An enlarged and updated internally consistent dataset with uncertainties and correlations:the system K_2O–Na_2O–CaO–MgO–FeO–Fe_2O_3–Al_2O_3–TiO_2–SiO_2–C–H_2–O_2. J Metamorphic Petrol 8:89–124

Huckenholz HG, Yoder HS (1971) Andradite stability relations in the $CaSiO_3$-Fe_2O_3 join. Neues Jahrb Mineral Abh 114:246–280

Huckenholz HG, Schairer JF, Yoder HS Jr (1969) Synthesis and stability of ferri-diopside. Mineral Soc Am Spec Pap 2:163–177

Hugh-Jones DA, Woodland AB, Angel RJ (1994) The structure of high-pressure C2/c ferrosilite and crystal chemistry of high-pressure C2/c pyroxenes. Am Mineral 79:1032–1041

Johnson RE, Muan A (1967) Activity-composition relations in solid solutions of the system CaO–"FeO"–SiO_2 in contact with metallic iron at 1080°C. Trans Metal Soc AIME 239:1931–1939

Köhler TP, Brey GP (1990) Calcium exchange between olivine and clinopyroxene calibrated as a geothermometer for natural peridotites from 2 to 60 kbar with applications. Geochim Cosmochim Acta 54:2375–2388

Koziol AM (1990) Activity-composition relationships of binary Ca–Fe and Ca–Mn garnets determined by reversed, displaced equilibrium experiments. Am Mineral 75:319–327

Lindsley DH (1967) The join hedenbergite-ferrosilite at high pressures and temperatures. Carnegie Inst Washington Yearbook 64:230–232

Lindsley DH (1980) Phase equilibria of pyroxenes at pressures > 1 atmosphere. In:Prewitt CW (ed) Pyroxenes:(Reviews in Mineralogy, vol 7): Mineral Soc Am, Washington, DC, 289–308

Lindsley DH (1981) The formation of pigeonite on the join hedenbergite-ferrosilite at 11.5 and 15 kbar:experiments and a solution model. Am Mineral 66:1175–1182

Lindsley DH, Munoz JL (1969) Subsolidus relations along the join hedenbergite-ferrosilite. Am J Sci 267-A:295–324

Liou JG (1974) Stability relations of andradite-quartz in the system Ca–Fe–Si–O–H. Am Mineral 59:1016–1025

Lucas H, Muggeridge MT, McConchie DM (1989) Iron in kimberlitic ilmenites and chromian spinels:a survey of analytical techniques. In:Ross J (ed) Kimberlites and related rocks, vol 2, Geol Soc of Aust Spec Publ, Blackwell, Australia, pp 311–319

Luth RW, Virgo D, Boyd FR, Wood BJ (1990) Ferric iron in mantle-derived garnets, implications for thermobarometry and for the oxidation state of the mantle. Contrib Mineral Petrol 104:56–72.

Massalski TB, Murray JL, Bennett LH, Baker H (1986) Binary alloy phase diagrams, Am Soc Met, Metals Park, Ohio, USA, pp 24–26.

Moecher DP, Essene EJ, Anovitz LM (1988) Calculation and application of clinopyroxene–garnet–plagioclase–quartz geobarometers. Contrib Mineral Petrol 100:92–106

Ohashi Y, Burnham CW, Finger LW (1975) The effect of Ca-Fe substitution on the clinopyroxene crystal structure. Am Mineral 60:423–434

Robie RA, Bin Y, Hemingway BS, Barton MD (1987) Heat capacity and thermodynamic properties of andradite garnet $Ca_3Fe_2Si_3O_{12}$, between 10 and 1000 K and revised values for $\Delta_f G^\circ_m$(298.15 K) of hedenbergite and wollastonite. Geochim Cosmochim Acta 51:2219–2224

Ross II CR, Armbruster T, Canil D (1992) Crystal structure refinement of a spinelloid in the system Fe_3O_4-Fe_2SiO_4. Am Mineral 77:507–511

Roth RS, Dennis JR, McMurdie HF (1987) Phase diagrams for ceramisists, vol VI. Am Ceram Soc, Westerville, Ohio, USA, pp 454–456

Schwartz KB, Nolet DA, Burns RG (1980) Mössbauer spectroscopy and crystal chemistry of natural Fe-Ti garnets. Am Mineral 65:142–153

Sueno S, Kimata M, Prewitt CW (1984) The crystal structure of high clinoferrosilite. Am Mineral 69:264–269

Suwa Y, Tamai Y, Naka S (1976) Stability of synthetic andradite at atmospheric pressure. Amer Mineral 61:26–28

Taylor BE, Liou JG (1978) The low temperature stability of andradite in C-O-H fluids. Am Mineral 63:378–393

Wood BJ, Nicholls J (1978) The thermodynamic properties of reciprocal solid solutions. Contrib Mineral Petrol 66: 389–400

Woodland AB, O'Neill HStC (1993) Synthesis and stability of $Fe_3^{2+}Fe_2^{3+}Si_3O_{12}$ garnet and phase relations with $Fe_3Al_2Si_3O_{12}$–$Fe_3^{2+}Fe_2^{3+}Si_3O_{12}$ solutions. Am Mineral 78:1000–1013

Woodland AB, Ross II CR (1994) A crystallographic and Mössbauer spectroscopy study of $Fe_3Al_2Si_3O_{12}$-$Fe_3^{2+}Fe_2^{3+}Si_3O_{12}$ (almandine–skiagite) and $Ca_3Fe_2^{3+}Si_3O_{12}$–$Fe_3^{2+}Fe_2^{3+}Si_3O_{12}$ (andradite–skiagite) garnet solid solutions. Phys Chem Miner 21:117–132

Zhang Z, Saxena SK (1991) Thermodynamic properties of andradite and application to skarn with coexisting andradite and hedenbergite. Contrib Mineral Petrol 107:255–263